Heliyon

ELSEVIER

Received:
5 October 2018
Revised:
8 January 2019
Accepted:
1 April 2019

Cite as: Anjan Roy, Arun B. Inamdar. Multi-temporal Land Use Land Cover (LULC) change analysis of a dry semi-arid river basin in western India following a robust multi-sensor satellite image calibration strategy. Heliyon 5 (2019) e01478. doi: 10.1016/j.heliyon.2019.e01478

Multi-temporal Land Use Land Cover (LULC) change analysis of a dry semi-arid river basin in western India following a robust multi-sensor satellite image calibration strategy

Anjan Roy*, **Arun B. Inamdar**

Centre of Studies in Resources Engineering, Indian Institute of Technology Bombay, Powai, Mumbai-400076, Maharashtra, India

* Corresponding author.

E-mail address: anjanrroy@gmail.com (A. Roy).

Abstract

Multi-temporal and multi-sensor satellite data calibration is an inherent problem in remote sensing-based applications. If multiple satellite scenes cover the study area, it is difficult to compare and process the images for change detection and long-term trend analysis of the same day and/or seasons from different satellites or sensors. Moreover, the validation of all the past images is a challenge due to unavailability of past ground truth datasets. The proposed calibration paradigm in this study is based on radiance normalization in the spatial and spectral domain to ease the alignment of multiple images into an identical radiometric foundation. In this study, an intuitive radiometric correction technique (at a daily, monthly and yearly scale) was proposed, aimed at all Landsat sensors' datasets for long-term Land Use Land Cover (LULC) trend analysis for a dry semi-arid river basin in western India, facing drought conditions. The post-calibration mosaiced images were smooth, and meaningful LULC classification results could be obtained easily for all the years. The LULC change dynamics were analyzed and compared for the years 1972, 1980, 1991, 2001, 2011 and 2016 in Shivna River

https://doi.org/10.1016/j.heliyon.2019.e01478

Basin. During these study periods, wasteland was found to be the most altered class, followed by agricultural land and forest. The spatial extent of agricultural land was found to decrease linearly, while forest cover showed an exponential decrease; a linear increase was observed in wasteland. Though during the 44 years study period (1972−2016), 241.48 km^2 area was converted to agricultural land from wasteland, but more than double that land was converted to wasteland from agricultural land; alarmingly, 5.18% (8.12% in 1972 and 2.94% in 2016) forest cover decreased. The existing forest cover in 2016 is approximately one-third compared to 1972. The present work provides a generic framework for the calibration of multi-temporal and multi-sensor satellite images for long-term LULC trend analysis, which can be adopted for other satellite datasets.

Keywords: Environmental science, Geophysics

1. Introduction

Land Use Land Cover (LULC) changes and climatic change in conjunction with soil deterioration alter the hydrological cycle, thereby progressively degrading the ecosystem and reducing the quality of land resources, biodiversity and agriculture (Bajocco et al., 2012). Due to rapid industrialization and increasing demographic pressure in India, natural resources are being over-exploited, precipitating a critical resource management challenge with shrinking agricultural lands and a rise in wasteland and hydrological crisis (Government of India, Ministry of Agricuture and Farmers Welfare: Deparment of Agriculture, 2016). The field area chosen for this study is one of the critical climate vulnerable hot semi-arid zones of India (approximately $1/4^{th}$ of the Aurangabad district, which is part of the Maharashtra State in western India). The study area is semi-arid in nature and is marked by very low summer monsoon rainfall (2012−2015), with low ground water table and water-stressed agricultural activity (Ratna, 2012). Studies have indicated that semi-arid regions are particularly stressed due to the combined effects of a burgeoning population and climate change (Mukherjee et al., 2009). A large portion of the study area is dependent on dams and surface water bodies to support basic farming practices. However, erratic summer monsoon and drought conditions in the past years dried up the accessible surface water sources and lowered the water levels in existing dam and reservoirs, thereby lowering agricultural productivity. A social crisis emerged in this backdrop with several farmers committing suicides in the last few years. In December 2015, the Union Government of India sanctioned financial relief to the tune of US $ 437.182 million to the entire Maharashtra State to fight against the drought challenge (Drought relief fund, 2015). Given such a scenario, it is vital to aid rapid and informed decision-making to ensure sustainable management of surface water, agricultural land, and reserved forest. Multi-temporal satellite image

https://doi.org/10.1016/j.heliyon.2019.e01478

analysis emerges as a potential solution, aiding the government as well as the farmers in chalking out a route-map for a given year with the available resources. Hence, continuous satellite-based multi-temporal monitoring is essential to estimate available surface water accessibility and its temporal fluctuations, and map the extent of agricultural land, forest cover and wasteland. It also helps in understanding their periodical changing trend to realize the aforementioned purpose, which is the final intended outcome of the entire research work.

There are several challenges in applying multi-temporal imagery to derive long-term LULC change detection on the earth's surface. The operation of Landsat Multispectral Scanner (MSS) to Landsat Operational Land Imager (OLI) sensors has led to a surge in spatial, spectral and temporal resolution change, which makes these data appropriate for investigating both rapid and steady changes in vegetation cover and monitoring of environmental processes (Gong et al., 2008). However, one major limitation is the difficulty in obtaining identical multi-temporal Landsat datasets that are comparable despite their different acquisition periods. Additionally, multi-temporal Landsat images are influenced by different sources of noise, related to the stability of sensors, changes in satellite responsivity, changes in illumination and atmospheric interferences (Vicente-Serrano et al., 2008). Kindu et al. (2013) analyzed LULC fluctuations in the landscape of Munessa-Shashemene area of the Ethiopian highlands over a period of 39 years from Landsat MSS, Thematic Mapper (TM) and Enhanced Thematic Mapper+ (ETM +) dataset. Likewise, calibration of multiple datasets was performed by Hansen and Loveland (2012) and Gómez et al. (2016). Zhu et al. (2016) monitored the greenness trends based on Landsat 5, 7, and 8 images. In addition, various algorithms were introduced for distinguishing land cover change by evaluating multi-temporal satellite data. Hence, integration of geographical information system and remote sensing data, change vector analysis, image differentiation etc. have emerged as significant techniques for change detection applications (Haque and Basak, 2017). Given its vital significance, the upgradation of the existing knowledge of radiometric calibration with all the available Landsat sensors' images is clearly indicated. Hence, the same has been attempted in the current research, bringing images from different sensors on a single platform to obtain meaningful classification results. The overall accuracy of LULC classification is 91.36% and the kappa index of agreement is 0.91, which is remarkable for a medium-sized study area such as this in a long duration (44 years) study. Otherwise, without the calibration process, the classification results are likely to be sub-standard and/or erroneous.

Inspired from the above considerations, this paper describes a unique calibration framework, which performs calibration and correction simultaneously at different temporal scales followed by LULC map preparation and long-term change detection. The noteworthy contributions of this paper have been summarized as:

https://doi.org/10.1016/j.heliyon.2019.e01478

i) In contrast to previous approaches for LULC classification for multi-temporal images, an effective radiometric correction technique is introduced, considering the temporal aspect on daily, monthly and yearly basis for a given date.

ii) Further, in order to ensure coherency in the LULC classification for all the images in the sequence, historic ground truth data (for accuracy assessment) for all the successive years of the used satellite images need to be checked; however, such datasets are usually not available. Hence, it is required to have proper use of multi-temporal and multi-sensor images with effective spectral and spatial calibrations.

iii) Since single sensor's dataset is not available for a long period, there is a need to use datasets from multiple sensors. It further emphasizes the need to adjust the images from multiple sensors onto the same platform for uniform analysis. Hence, the latest image (February 2016) was calibrated with all other images on a single platform, and the LULC analysis was cross-validated.

iv) We provide extensive quantitative and qualitative assessments for analyzing long-term changes in the considered study area. In particular, we have shown inter-class thematic changes, apart from producing land-cover maps through an active learning-based hybrid classification system.

2. Study area

Shivna river is one of the major tributary of upper Godavari river in Aurangabad district of Maharashtra, western India. The area chosen for this study is Shivna River Basin (Fig. 1), which is an important sub-basin of Upper Godavari River Basin mainly in Aurangabad district of northwestern part of Maharashtra. It covers 2610 km^2 area and lies between latitude 19°35′N to 20°20′N and longitude 74°44′E to 75°18′E. The basin is under Sub-tropical Deccan Plateau Hot Semi-Arid Eco-Region 6.2 of Agro Ecological Sub Region (Indian Council of Agricultural Research) and Western Plateau and Hills Region (IX) and Western Maharashtra Scarcity Zone (MH-6) of Agro Climatic Region (by National Agricultural Research Project) receiving reasonable to low rainfall. The rainy season begins from June and lasts until the end of September (Ratna, 2012). Most of the area i.e. more than 80% falls in low rainfall (less than 600 mm) zone. In this area, 68% rainfall occurs due to southwest monsoon during June to September and the remaining 5% occurs after December. Drought in the study area is a common phenomenon and it distresses the area to a varying magnitude. The study area and entire Aurangabad district experienced many severe droughts that have devastated previously like other parts of Maharashtra. The farming yield of this area is not only sensitive to temperature rises, but also depends on the changes in the nature and characteristics of summer monsoon. Cotton, maize, pearl millet, pigeon pea, sorghum and sugarcane are the main rainfed kharif (monsoon) crops and wheat, gram, safflower and groundnut are the main rabi

https://doi.org/10.1016/j.heliyon.2019.e01478

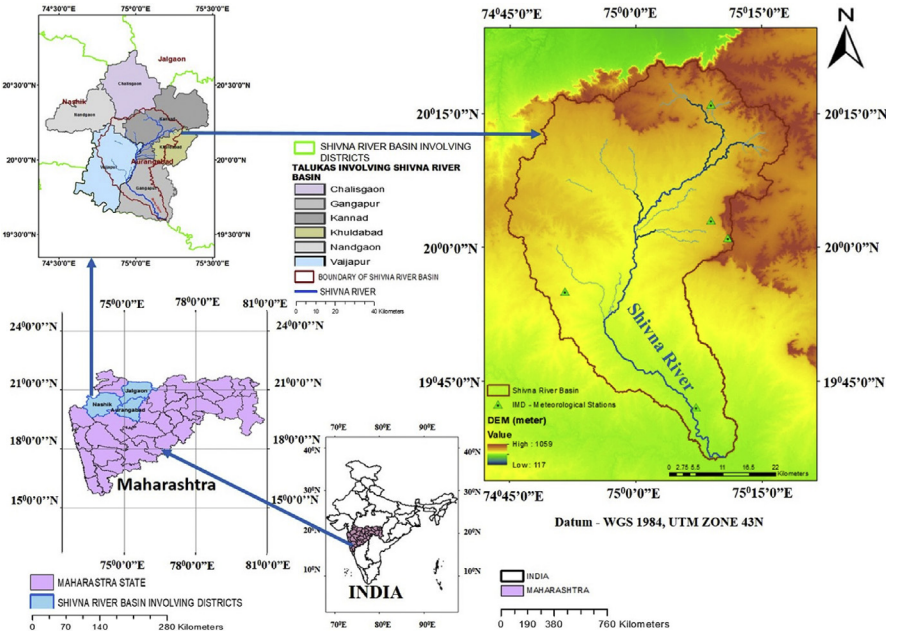

Fig. 1. Geographical location map of the Shivna River Basin.

(post monsoon) crops cultivated at this region (Bodh et al., 2016). Local climatic conditions and natural disaster like drought, influence the spatial occurrence of surface water bodies (naturally occurring lakes and constructed dams etc.) and agricultural landscape of the Shivna River Basin.

3. Materials and methods

3.1. Dataset

All Landsat sensors' images were selected for the analysis, including Landsat MSS to OLI images (acquired from November 14, 1972 to February 19, 2016; approximately in decadal interval) for this study, given that long-term monitoring is required and the study area is local and moderate in magnitude. Landsat satellite images (Table 1) were obtained from the USGS Global Visualization Viewer (http://glovis.usgs.gov/) dataset, which has L1T characteristics for the years 1972, 1980, 1991, 2001, 2011 and 2016. Images were mostly selected from the post-monsoon season (rabi season, February month) with ample agricultural and vegetation growth and filled water bodies. Good quality images with less than 10% cloud cover were obtained. The DEM (Digital Elevation Model, 30 meter spatial resolution) was acquired from [Advanced Spaceborne Thermal Emission and Reflection Radiometer (ASTER) Global Digital Elevation Model (GDEM)] http://gdem.ersdac.jspacesystems.or.jp/. The features of the used satellite images and DEM are given in Table 1. All the Ground Control Points (GCPs) were collected during the field visit in February 2016 through the interpretation of Survey of India (SoI, 1:50,000

https://doi.org/10.1016/j.heliyon.2019.e01478

Table 1. Details of satellite images and other datasets used in the study.

Satellite	Meta Data			
	Sensor	**Date of Image Acquisition**	**Path/Row**	**Spatial Resolution**
Landsat1	MSS	1972-11-14	157/046	60m
Landsat 3	MSS	1980-04-06	157/046	60m
Landsat5	TM	1991-02-01 & 1991-02-10	147/046 &146/046	30m
Landsat7	ETM+	2001-02-20 & 2001-04-02	147/046 &146/046	30m
Landsat5	TM	2011-02-08 & 2011-02-01	147/046 &146/046	30m
Landsat8	OLI	2016-02-15 & 2016-02-06	147/046 &146/046	30m
ASTER GDEM			Resolution: 30m	
Topographic map (SoI)	Surveyed in 1973−1974		(Scale - 1:50000) (Published in 1975)	
Google Earth	2018		(Varying resolution)	

scale) topographic maps and Google earth. Field verification was ensured with a GPS device to collect the exact longitude and latitude, covering major parts of the study area. All the datasets used in this study are available free-of-cost. Moreover, Normalized Difference Vegetation Index (NDVI) and Normalized Difference Water Index (NDWI) maps were prepared and used as additional layers for cross-validation and accuracy assessment to further enhance the classification results.

3.2. Methodology

Broadly, the proposed methodology consists of three major stages:

A. First, the images were pre-processed for outlier removal and further corrected for radiometric errors before moving to sensor calibration in the spatial domain.

B. In the next stage, image mosaicing were performed after the images were processed for atmospheric interferences. Since the spatial extent of mosaiced images contained excess area in comparison to the study area under consideration, the subset images were extracted highlighting the study area using DEM based watershed delineation technique.

C. Finally, hybrid classification was carried out for thematic LULC change analysis and the classifier performance is assessed based on well-known measures from the remote sensing literature.

The stages are further elaborated in the following sections and the glimpse of the overall methodology is illustrated in Fig. 2

https://doi.org/10.1016/j.heliyon.2019.e01478

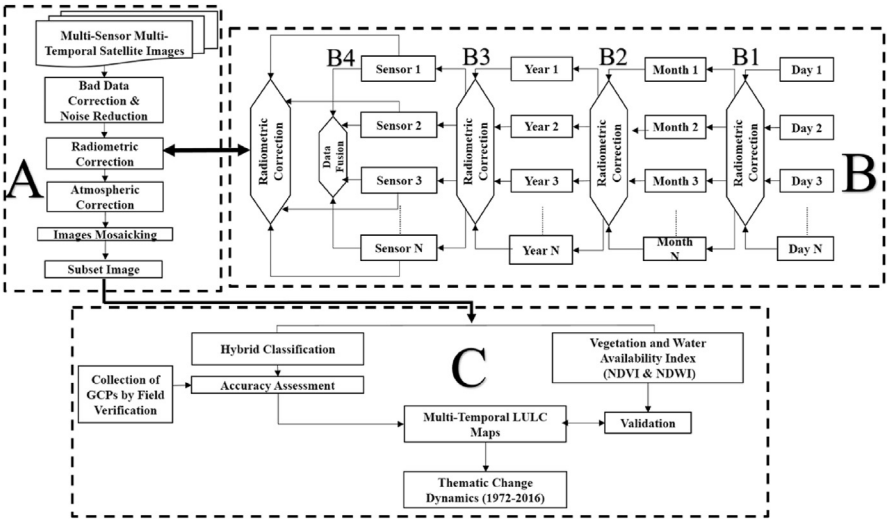

Fig. 2. Schematic framework of the proposed methodology.

3.2.1. Section A

3.2.1.1. Image pre-processing

Initially, geometric correction was accomplished using first-order polynomial transformation fit, while nearest neighbor algorithm was used to conduct the resampling procedure and the image-to-image registrations (Jensen and Lulla, 1987). The identified negative values were initially replaced with zero; further, the average pixel score obtained from a 3×3 neighborhood was taken as the minimum window size for over smoothing. Finally, negative values were replaced with the calculated average pixel value.

3.2.1.2. Radiometric corrections of multi-sensor and multi-temporal datasets

There are variations in terms of dimensionality of the obtained dataset, which consists of diurnal, seasonal, monthly and yearly time spans; they need to be analyzed and registered uniformly to compare the change detection. First, the data of a single sensor in daily, monthly and yearly scale was calibrated, and this step was repeated for all the sensors. However, in the case of LULC trend analysis for a vast river basin, the entire study area is unlikely to be captured in a single satellite image scene. Hence, multiple images are needed to cover the whole area, and these images are generally not captured by one sensor at a single time. The available data consists of changes in the monthly as well as daily scale. Hence, it is essential to calibrate radiometric responses at a single level. The overlapping areas in the images of multiple scenes are identified to calibrate the radiometric response of the different days and/or months of the data. Broadly, three cases are possible in this respect:

https://doi.org/10.1016/j.heliyon.2019.e01478

i) The overlapped portion of the images contains a land cover class, which has remained invariant to any kind of change at the temporal scale. Specifically, such is the case in this study. This class was termed as the "static class".

ii) In case the aforementioned static class cannot be found, the calibration was performed for all the classes contained in the overlapped area.

iii) Further, if the multiple scenes were not overlapping, then the same technique as of the above two cases were repeated, but for the whole image area.

If the overlapping area includes all the classes present in the entire image, then the number of classes identified from the intersected area undergoes no changes for both the image scenes. In the current study, two scenes could sufficiently cover the study area selected. The average values for each class from both the images, followed by the gain values for different classes as the ratio of the average class values of both the images, were calculated. The obtained average class values for one image were further normalized by multiplying the gain with the corresponding class values of the other image. If both the images capture the overlapping area and do not contain all the classes present in the entire image, then a single object which was intact and present in both the images during the time period (for example, desert, roads, barren rock type or water bodies) was identified. Then, the identified average value of the object of the single area was calculated from both the images. Further, gain was calculated by dividing average value from image 1 to average value of image 2. Then, each of the pixel values of image 2 was multiplied by the gain. Correction was again essential for trend analysis and change detection during several periods of a single season, to minimize the difference of atmospheric effects in the yearly dataset. For the aforementioned purpose, the static area (for example, desert, unmetalled roads, water bodies, or barren rock type) was identified from all the yearly images and the same process was repeated.

3.2.1.3. Sensor's images calibration

Image registration is the way out to align multiple images with varied sensor specifications. The data fusion technique was used by highlighting the best required spatial resolution as a reference with respect to the other spatial resolution for calibration. For the calibration of different spectral resolutions of the different sensors' images, initially the bands of corresponding wavelengths containing maximum common value of the range of wavelengths were identified. The stages relating to the static area localization were followed in the identical fashion. Further, the average radiometric response from the identified static area for a single sensor was calculated. The range values corresponding to the matching bands in different images were first brought into similar scale with reference to the wavelength range of the most required sensor (2016 image, Landsat OLI in the current scenario). The gain values for different sensors were calculated by dividing the average radiometric value of the

https://doi.org/10.1016/j.heliyon.2019.e01478

required sensor to the average radiometric value of the remaining sensors. The corresponding gain values were multiplied with the corresponding sensor's radiometric value of the whole bands. Identical steps were repeated for the other bands as well.

3.2.2. Section B: Atmospheric correction, image mosaicing and image subset

Atmospheric corrections for the remote sensing data are mainly done based on image statistics, empirical methods and the radiative transfer model. There are several atmospheric correction tools, which can be applied in this respect. However, a radiative transfer model-based Fast Line-of-sight Atmospheric Analysis of Hypercubes (FLAASH) tool in ENVI 5.0 was considered for the same. Since a single Landsat scene does not cover the study area, it is required to obtain several scenes to achieve the purpose. Several satellite image processing software are available wherein image mosaicing can be performed. Here, a georeferenced pixel-based image mosaicing tool in ENVI 5.0 was applied. After mosaicing, the images may contain extended pixels, which were beyond the study area. For this purpose, a DEM-based watershed delineation technique was performed for subset area detection and the images subset was prepared using the obtained watershed outline.

3.2.3. Section C: Detailed analysis

Integrated hybrid classification technique, which comprises of unsupervised and supervised classification techniques, was applied combined with human knowledge. Sometimes the classified groups are manifested by a salt-and-pepper appearance. Hence, post classification smoothing is required to obtain a smooth LULC map. Here, the visual interpretation technique was applied to obtain the final classified images. Ground truth data were obtained by visiting numerous locations throughout the study area, to ensure its adequate coverage. A GPS device (GARMIN eTex 20) was used to ensure accuracy of locations, which were collected and matched to the satellite dataset. Random sample points were collected from field verification as per the stratified sampling method combined with high resolution Google Earth images. Pixels (field-based samples) with the following distributions for different classes were collected - 266 pixels for agricultural land, 147 pixels for water, 241 pixels for wasteland, 123 pixels for forest and 84 pixels for built-up area from the field visit. The classification outcomes with the aforementioned pair of indices, i.e., NDVI and NDWI were cross-verified to obtain more consolidated LULC classification results. Finally, post-classification change detection technique was followed in the ENVI thematic change workflow tool to depict the LULC change dynamics in the Shivna River Basin during the periods of 1972−1980, 1980−1991, 1991−2001, 2001−2011, 2011−2016 and 1972−2016 (overall). Only altered

https://doi.org/10.1016/j.heliyon.2019.e01478

areas were taken into consideration for the change dynamics. Initially, twenty unique classes were introduced for interclass conversions. However, among these, built-up to water and water to built-up classes were eliminated due to insignificant/no conversion values to visualize.

4. Results

The multi-sensor images available from Landsat TM (in 1991 and 2011) and Landsat ETM^{+} (2001) containing common wavelength RGB bands were considered as the reference since they intersect for the maximum number of images in the sequence. Similar normalization was carried out for the Landsat OLI image (2016) and Landsat MSS images (1972 and 1980) as well. Further, in Landsat MSS images, the NIR band (0.76−0.90 μm) was scattered into two bands (Band 6: 0.70−0.80 μm and band 7: 0.80−1.1 μm), which were finally settled down within the above-mentioned NIR range. The final working bands were Green (0.52−0.60 μm), Red (0.63−0.69 μm), and Near Infra-Red (NIR: 0.76−0.90 μm) for all the sensors.

In Fig. 3, one identical random pixel was selected from all the images and its radiance property was shown in the radiance spectra, which were plotted against the wavelength for selected yearly datasets before and after calibration.

It was observed that after the calibration process, the single pixel data from all the years became nearly coherent, whereas before calibration, the radiance spectra varied randomly. The reflectance data was rescaled into 0 to 10000 for better discrimination and quantification, simple visualization and for occupying less memory for further processing. The negative reflectance values (Fig. 4) indicate that the

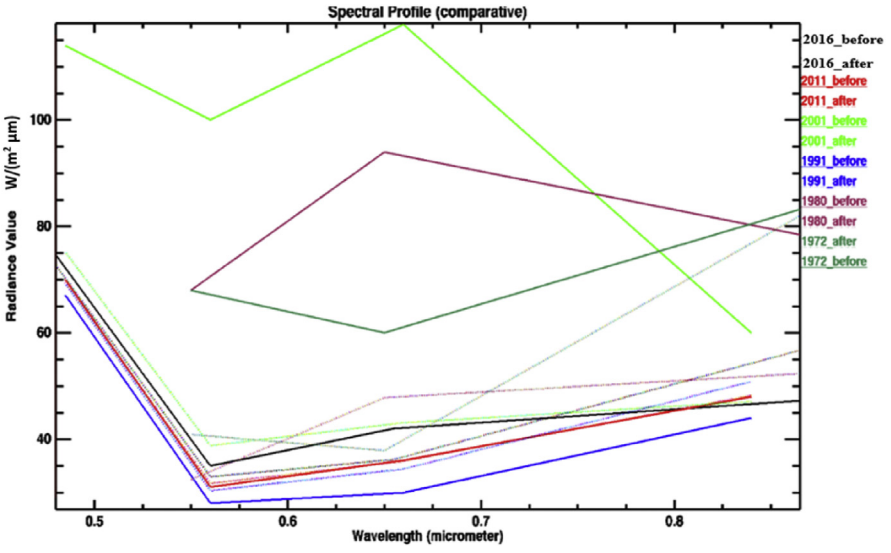

Fig. 3. Radiance values of images before (solid lines) and after corrections (dotted lines) for the years 1972, 1980, 1991, 2001, 2011 and 2016.

https://doi.org/10.1016/j.heliyon.2019.e01478

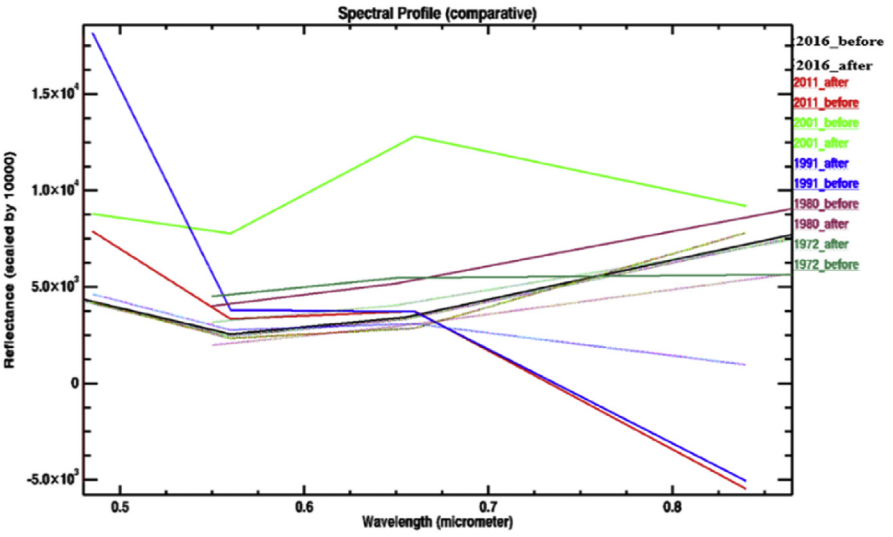

Fig. 4. Reflectance values of images before (solid lines) and after corrections (dotted lines) for the years 1972, 1980, 1991, 2001, 2011 and 2016.

corresponding pixels come from invalid data points. Therefore, noise reduction and calibration was much essential before converting radiance into reflectance values.

Before correction, pattern noise such as stripes and bad sectors, which disappeared after noise correction and de-stripping were evidently noticeable in the 1980 image (Fig. 5). In addition, different parts of the images clearly showed brightness difference in the 1991, 2001 and 2011 images after mosaicing, which disappeared after applying the proposed methodology. The images from 1991, 2001 and 2011 became completely smooth after the processing and were ready to undergo the next step. Finally, in order to obtain a uniform spatial characteristic, the images in 1972 and 1980 were pan-sharpened and super-resolved to obtain a spatial resolution of 30m (similar to 1991, 2001, 2011, and 2016) from 60m.

4.1. LULC classification and trend analysis for the Shivna River Basin

Five major LULC classes were identified, namely, Agricultural land, Water, Wasteland, Forest and Built-up area, for the LULC classification purpose. The agricultural land included major crop-sown area and cultivable lands with patches and croplands in pattern. Water included natural water bodies, small to medium reservoirs, canals and dams. Wasteland included very minimum vegetation to bare soil, dry lands and rocks. Forest included mainly reserved forests, with medium to high density of plant growth, while built-up area included small villages. In this section, the Shivna River Basin was selected as the study area, and the study period covered the last 44 years (1972−2016). Agricultural land, surface water, wasteland and forest area trend analysis are shown in Fig. 6 and Table 2.

https://doi.org/10.1016/j.heliyon.2019.e01478

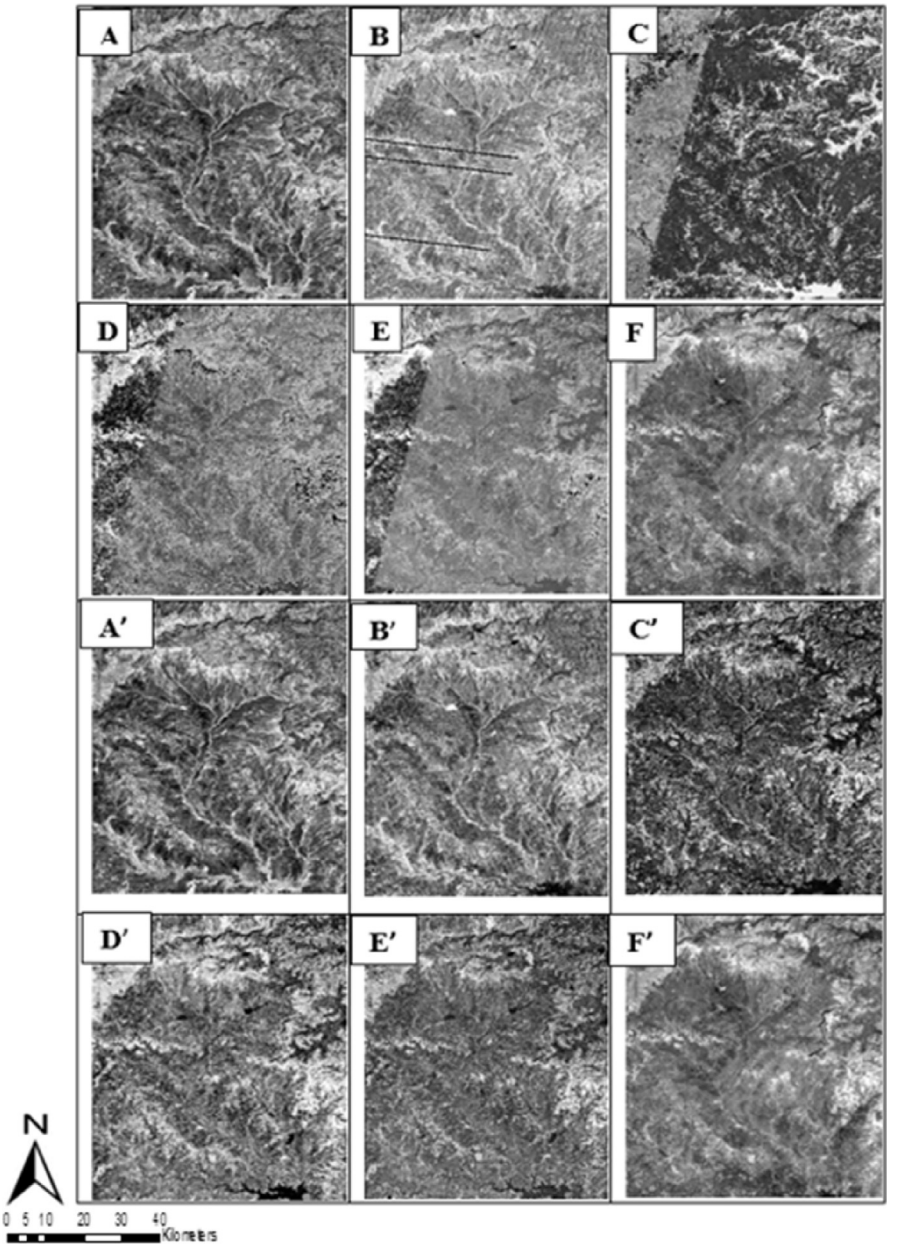

Fig. 5. A-F are the images from 1972, 1980, 1991, 2001, 2011 and 2016, respectively before the noise and radiometric calibration. A′-F′ are the images from 1972, 1980, 1991, 2001, 2011 and 2016, respectively after the noise and radiometric calibration.

4.2. Accuracy assessment and validation of LULC maps

4.2.1. Error matrix and kappa coefficient-based accuracy assessment

The confusion matrix-based accuracy assessment (Congalton, 1991) and Kappa coefficient were considered for assessing the performance of the classification

https://doi.org/10.1016/j.heliyon.2019.e01478

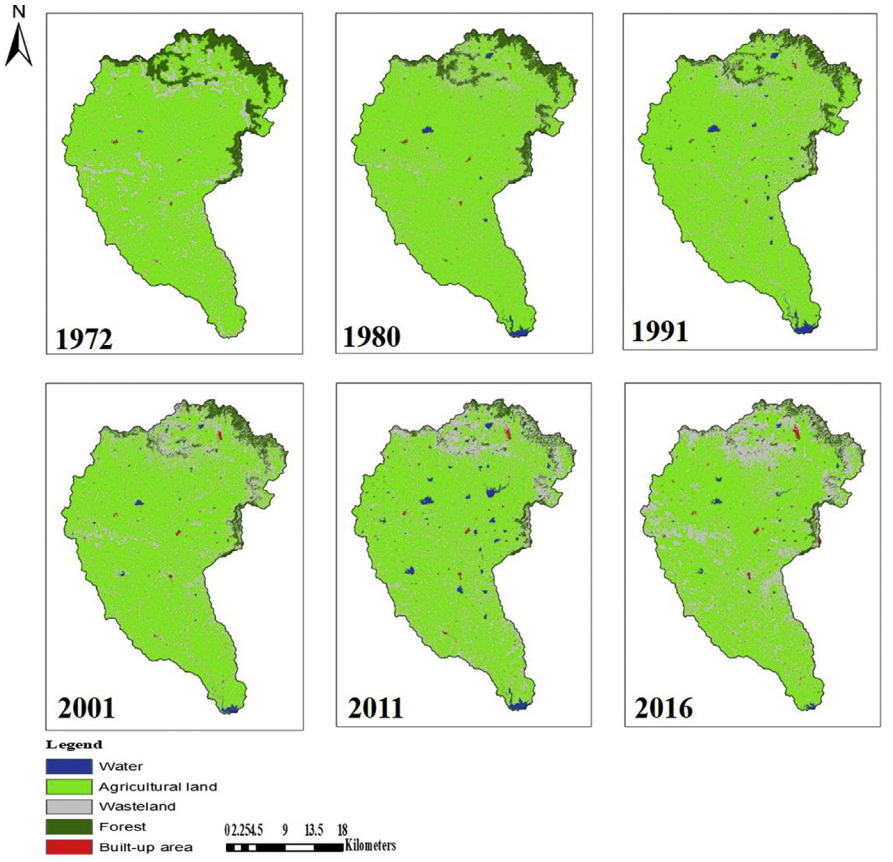

Fig. 6. LULC changes in the Shivna River Basin in 1972, 1980, 1991, 2001, 2011 and 2016.

system (Rogan and Chen, 2004). It is difficult to carry out accuracy assessment for all the classified LULC maps (except current) due to a lack of past ground truth data. Therefore, any recent OLI-based accuracy assessment represents the overall accuracy measure for all the classified maps as all the datasets were calibrated on a single platform. 839 random sample points belonging to all the corresponding LULC classes were selected through the stratified sampling method and verified against the reference data. The results showed an overall accuracy of 91.36% and kappa index of agreement value of 0.91. The accuracy levels for Agricultural land, Water, Wasteland, Forest and Built-up area were 89.85%, 92.7%, 92.53%, 90.17% and 91.57%, respectively. All classes were over 90% in terms of class-wise accuracy except the agricultural land. Similar accuracy levels are expected from the past LULC maps with very little deviation. It is evident that the present classification approach has been effective in producing consistent results irrespective of differences in spatial, spectral and radiometric resolution of satellite images from the accuracy assessment.

https://doi.org/10.1016/j.heliyon.2019.e01478

Table 2. Multi-temporal LULC change matrix of the Shivna River Basin.

Year	% Agricultural land	Area (km^2)	% Forest	Area (km^2)	% Water	Area (km^2)	% Waste land	Area (km^2)	% Built-up Area	Area (km^2)
1972	75.42	1985.06	8.12	213.72	0.05	1.29	16.23	427.17	0.20	5.27
1980	74.33	1956.37	6.35	167.13	0.73	19.16	18.35	482.97	0.25	6.53
1991	72.94	1919.78	5.47	143.97	1.18	31.03	20.12	529.56	0.31	8.03
2001	69.77	1836.35	4.23	111.33	0.55	14.32	25.11	660.90	0.36	9.51
2011	65.41	1721.60	3.05	80.28	1.88	49.48	29.22	769.07	0.45	11.87
2016	63.69	1676.32	2.94	77.39	0.57	15.08	32.25	848.82	0.56	14.61

4.2.2. Cross-validation based on NDVI & NDWI

NDVI (Rouse et al., 1974) and NDWI (McFeeters, 1996) analysis was carried out for the current Landsat OLI data in 2016 (Fig. 7). The NDVI scores were thresholded to distinguish vegetation from non-vegetation areas effectively. A threshold value of 0.2 was taken into consideration based on the ground knowledge, and was further used to detect changes. The LULC map (2016) was validated with ground truth accuracy, and further cross-validated using the maps obtained from the NDVI-NDWI measures. In the current study, it was observed that the results obtained from the calibrated images matched more closely with the maps obtained from the NDVI-NDWI measures. These results further establish the need for robust calibration before carrying out the classification task.

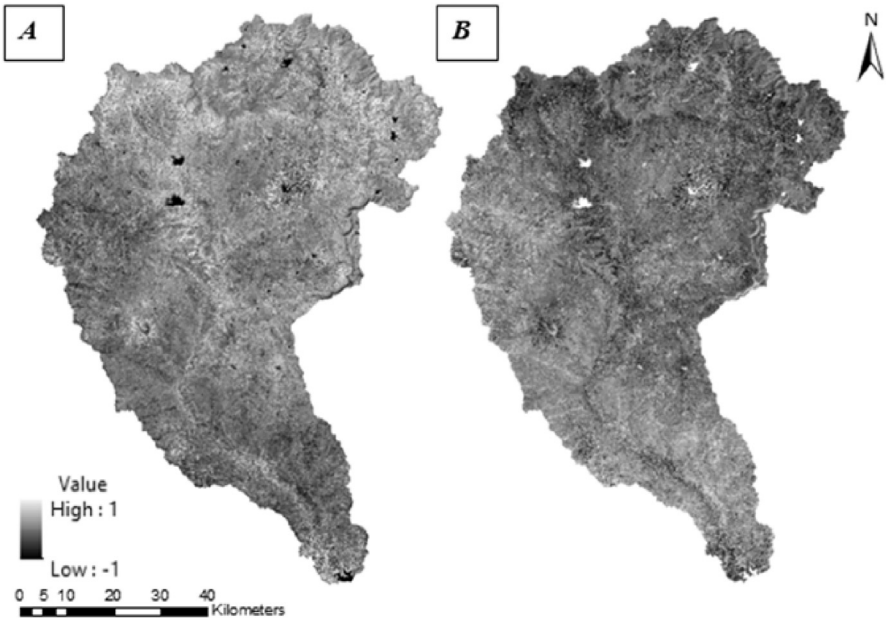

Fig. 7. (A) NDVI and (B) NDWI images with Landsat OLI image (February 2016) of the Shivna River Basin.

https://doi.org/10.1016/j.heliyon.2019.e01478

5. Discussion

Fig. 8 and Table 2 illustrate the quantitative changes in LULC classes (agricultural land, forest, water, wasteland and built-up area) to the corresponding years 1972, 1980, 1991, 2001, 2011 and 2016, respectively. The decrease in agricultural land was by 1.09%, 1.39%, 3.17%, 4.36% and 1.72% during 1972−1980, 1980−1991, 1991−2001, 2001−2011 and 2011−2016, respectively; the overall agricultural land decrease during the entire 44years period of 1972−2016 was 11.73% with an annual decrease rate of 0.27%/year. The highest rate of decrease was 0.44%/year during the decade of 2001−2011 (overall decrease of 4.36%). The decrease in forest cover was 1.76%, 0.88%, 1.24%, 1.18% and 0.11% during 1972−1980, 1980−1991, 1991−2001, 2001−2011 and 2011−2016, respectively. The forest cover decreased approximately 5.18% (from 8.12% in 1972 to 2.94% in 2016) due to the recent change in monsoon pattern. The highest rate of decrease in forest cover was 0.22 %/year, observed during 1972−1980 (overall decrease of 1.77%). The change in water was 0.68%, 0.45%, -0.64%, 1.34% and -1.31%, respectively, during the afore-mentioned periods, whereas the increase in built-up area was 0.048%, 0.056%, 0.057%, 0.09% and 0.104%. However, the increase in wasteland area was most remarkable at 2.12%, 1.77%, 4.99%, 4.11% and 3.03% during 1972−1980, 1980−1991, 1991−2001, 2001−2011 and 2011−2016, respectively. The overall wasteland increase during 1972−2016 was 16.02% with a 0.37%/year rate, whereas the highest rate of increase was 0.61%/year during the period 2011−2016 (overall increase of 3.03%).

The most significant LULC conversion took place from agricultural land to wasteland, followed by wasteland to agricultural land and forest cover to wasteland. The spatial extent of wasteland increased at the cost of agricultural land, forest and water bodies (dams and natural water bodies) in the Shivna River Basin. During 1980−1991, the rate of wasteland conversion was rather low (0.16%/year). 240.3 km^2 area was converted to agricultural land from wasteland. However, more than double that area (534.89 km^2) was converted to wasteland from agricultural land;

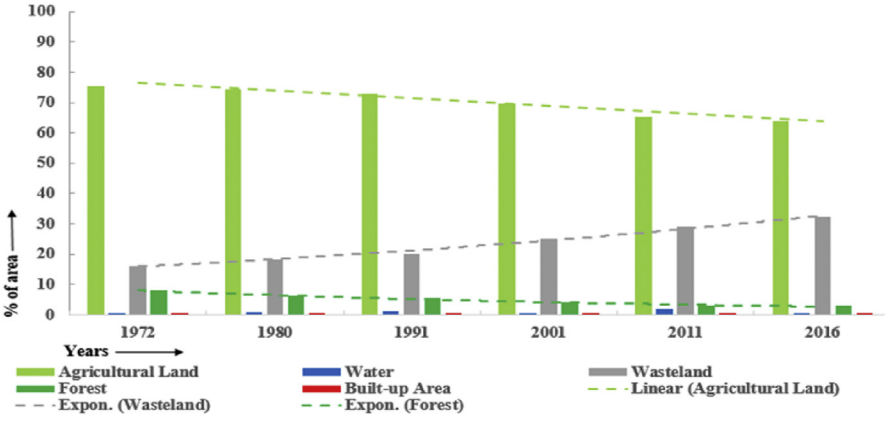

Fig. 8. Graphical representation of LULC changes in the Shivna River Basin.

https://doi.org/10.1016/j.heliyon.2019.e01478

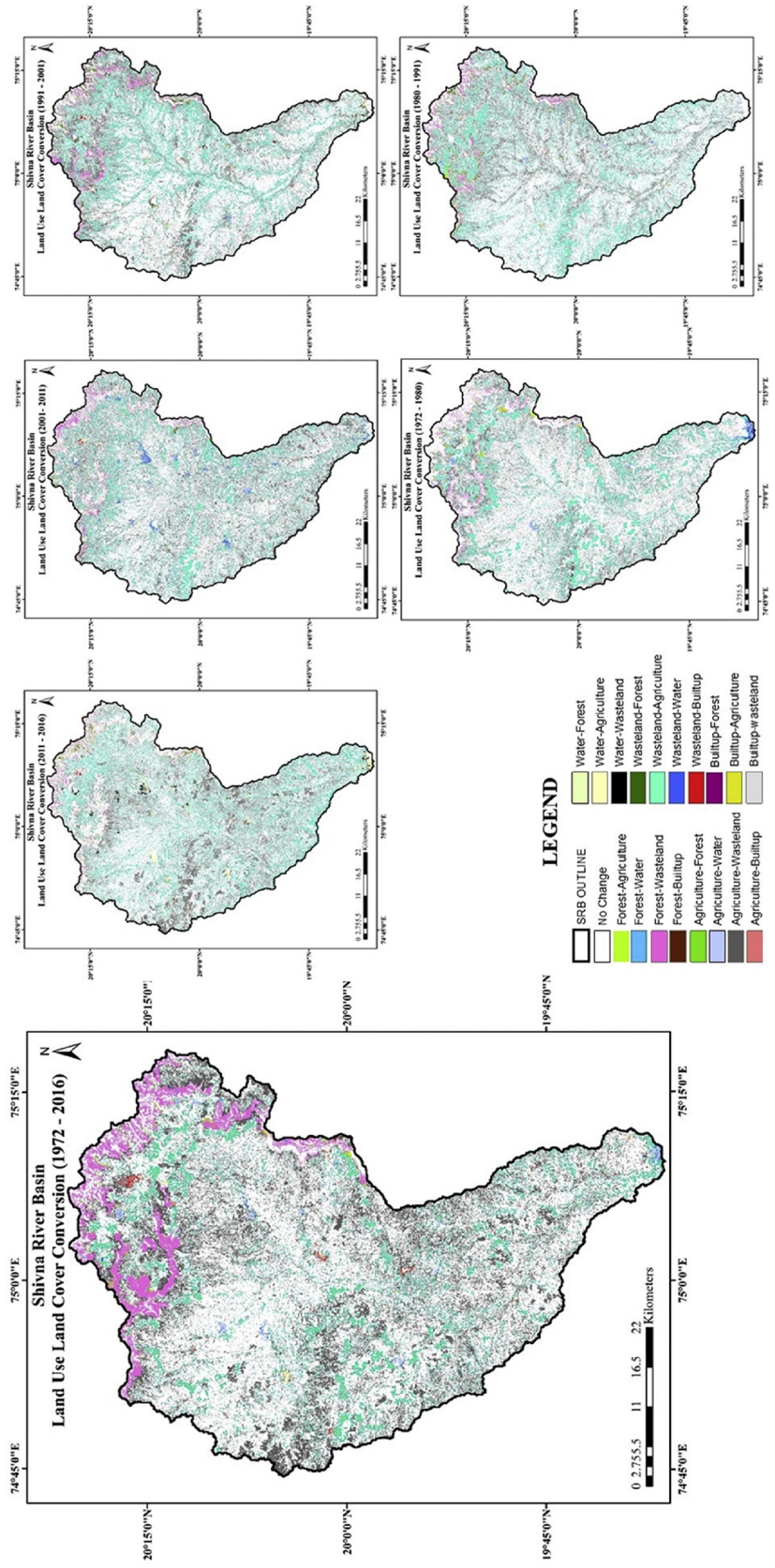

Fig. 9. Periodical thematic changes of the Shivna River Basin.

https://doi.org/10.1016/j.heliyon.2019.e01478

such conversions occurred in locations scattered throughout the study area, and were determined using thematic change analysis during the last 44 years (1972−2016). The existing forest cover in 2016 is approximately one-third compared to 1972 (213.33 km^2 in 1972 and 77.38 km^2 in 2016). These losses along with the increase in LULC area (decrease in agricultural land and forest cover and increase in wasteland) may be attributed to the recent erratic behavior of the monsoon and the ensuing drought scenario in the study area during 2012−2015. The varying pattern of the water bodies throughout the study area during 1972−2016 was also observed. The area covered by surface water increased in 1991 compared to the preceding decades, due to the construction of numerous dams during 1973−1990. The surface water bodies and dams were filled with water (may be observed from the classified images) in 1991 and 2011, due to ample mean yearly and monsoon rainfall; in 2011, it was the highest among all the years studied. The abundance of surface water was less in 2016 as compared to 2011 despite the construction of several dams, given the very low rainfall during the preceding drought years (2012−2015). In 1972, there was absence of water in the extreme southern part of the study area. After constructing the Jaikawadi-I dam in 1976, one may observe the image of a water body in the southern tip of the study area from the year 1980 onwards. Also, the growth of built-up area (0.008%/year, during 1972−2016) may be called sluggish given that the study area is mostly rural and agriculture-based and was affected by severe drought conditions. The thematic change analysis provides comprehensive knowledge about pixel conversion and class change about the converted landscapes dynamics. The study considers the valid classes that bring about substantial change resultant. It measures the transition dynamics of a LULC class to alternative class at a specified extent. An optional clean up or refine operation was performed after the execution to emphasize the result. Fig. 9 and Table 3 illustrate the total change scenario (1972−2016) with the conversion statistics of each class.

Table 3. Thematic aerial change statistics of the Shivna River Basin.

	Initial State (1972)	**Area (km^2)**					
Final State(2016)		**Forest**	**Agricultural land**	**Water**	**Waste land**	**Built-up Area**	**Row Total**
	Forest	75.08	5.58	0.54	131.62	0.51	213.33
	Agricultural land	0.42	1430.44	10.99	534.89	8.41	1985.17
	Water	0	0.13	1.11	0.06	0	1.3
	Wasteland	1.29	240.3	2.47	180.71	2.39	427.14
	Built-up Area	0	1.18	0	0.77	3.32	5.27
	Class Total	76.79	1677.63	15.11	848.05	14.63	0
	Class Change	1.71	247.19	14	667.34	11.31	0
	Image Difference	-136.54	-307.54	13.81	420.9	9.36	0

https://doi.org/10.1016/j.heliyon.2019.e01478

6. Conclusion

It is evident that remote sensing is a crucial trend analysis tool for multi-temporal LULC change. However, the availability of the remote sensing dataset from a single sensor, by a single scene for the trend analysis in a large-sized study area is doubtful. There is a need to use multi-temporal and multi-sensor images for analyzing the long-term changes that have taken place in the study area over time. However, the multi-sensor and multi-temporal satellite datasets contain different levels of noise, diverse atmospheric conditions and radiometric and spectral information. Hence, it is essential to bring all the datasets to a common denominator. In order to mitigate such flaws with multi-temporal and multi-sensor data, a novel approach was proposed in the present study to minimize radiometric differences and bring them within an acceptable range. Further, the technique was applied to perform LULC trend analysis and periodical change detection for the study area. The classified LULC maps could provide validated and accepted classification results with the calibrated dataset. The entire study was performed by exploiting all the Landsat sensors' images for long-term LULC monitoring and periodical change detection. This study is infrequent in the application domain of remote sensing. Moreover, the thematic change workflow assisted in observing the dynamics of the changing LULC classes within different periods in several possible prospects. The details of multi-temporal agricultural land, surface water fluctuations, wasteland and forest cover change trends, which were generated through the proposed methodology for the study area, can assist in policymaking and future LULC management. We plan to extend this study for dry semi-arid regions of the entire Maharashtra State in the near future with various satellite datasets.

Declarations

Author contribution statement

Anjan Roy: Conceived and designed the experiments; Performed the experiments; Analyzed and interpreted the data; Contributed reagents, materials, analysis tools or data; Wrote the paper.

Arun Inamdar: Wrote the paper.

Funding statement

This work was supported by the research grant (for teaching assistance) of Ministry of Human Resource Development (MHRD) through Indian Institute of Technology (IIT) Bombay and partial support of Industrial Research and Consultancy Centre (IRCC), IIT Bombay, India.

https://doi.org/10.1016/j.heliyon.2019.e01478

Competing interest statement

The authors declare no conflict of interest.

Additional information

No additional information is available for this paper.

Acknowledgements

The authors would like to thank United States Geological Survey (USGS) for disseminating the long-term Landsat satellite dataset.

References

Bajocco, S., De Angelis, A., Perini, L., Ferrara, A., Salvati, L., 2012. The impact of Land Use/Land Cover Changes on land degradation dynamics: a Mediterranean case study. Environ. Manage. 49, 980–989.

Bodh, P.C., Chaudhary, Sheela, J., Pant, N., Shrama, A., Yadav, M., Virmani, S., Pandey, R.S., Devi, S., 2016. Agricultural Statistics at a Glance, pp. 73–250.

Congalton, R.G., 1991. A Review of Assessing the Accuracy of Classifications of Remotely Sensed Data, vol. 46, pp. 35–46.

Gómez, C., White, J.C., Wulder, M.A., 2016. Optical remotely sensed time series data for land cover classification: a review. ISPRS J. Photogramm. Remote Sens.

Gong, J., Sui, H., Ma, G., Zhou, Q., 2008. A review of multi-temporal remote sensing data change detection. Int. Arch. Photogramm. Remote Sens. Spat. Inf. Sci. XXXVII (B7), 757–762. Beijing 2008 37.

Government of India, Ministry of Agricuture and Farmers Welfare: Deparment of Agriculture, C. And W., 2016. India Annual Report 2016-17, p. 194.

Hansen, M.C., Loveland, T.R., 2012. A review of large area monitoring of land cover change using Landsat data. Remote Sens. Environ. 122, 66–74.

Haque, I., Basak, R., 2017. Land cover change detection using GIS and remote sensing techniques: a spatio-temporal study on Tanguar Haor, Sunamganj, Bangladesh. Egypt. J. Remote Sens. Sp. Sci. 20, 251–263.

Jensen, J.R., Lulla, K., 1987. Introductory digital image processing: a remote sensing perspective. Geocarto Int. 2, 65.

Kindu, M., Schneider, T., Teketay, D., Knoke, T., 2013. Land use/land cover change analysis using object-based classification approach in Munessa-Shashemene landscape of the ethiopian highlands. Rem. Sens. 5, 2411–2435.

https://doi.org/10.1016/j.heliyon.2019.e01478

Maha [WWW Document], n.d. . December 30 Drought Relief Fund worth Rs 5,083 Cr for MP, 2015. URL. http://www.freepressjournal.in/drought-relief-fund-worth-rs-5083-cr-for-mp-maha/746014.

McFeeters, S.K., 1996. The use of the Normalized Difference Water Index (NDWI) in the delineation of open water features. Int. J. Remote Sens. 17, 1425–1432.

Mukherjee, S., Shashtri, S., Singh, C.K., Srivastava, P.K., Gupta, M., 2009. Effect of canal on land use/land cover using remote sensing and GIS. J. Indian Soc. Remote Sens. 37, 527–537.

Ratna, S.B., 2012. Summer monsoon rainfall variability over Maharashtra, India. Pure Appl. Geophys. 169, 259–273.

Rogan, J., Chen, D., 2004. Remote sensing technology for mapping and monitoring land-cover and land-use change. Prog. Plann. 61, 301–325.

Rouse, W., Haas, R.H., Deering, D.W., 1974. Monitoring Vegetation Systems in the Great Plains with ERTS.

Vicente-Serrano, S.M., Pérez-Cabello, F., Lasanta, T., 2008. Assessment of radiometric correction techniques in analyzing vegetation variability and change using time series of Landsat images. Remote Sens. Environ. 112, 3916–3934.

Zhu, Z., Fu, Y., Woodcock, C.E., Olofsson, P., Vogelmann, J.E., Holden, C., Wang, M., Dai, S., Yu, Y., 2016. Including land cover change in analysis of greenness trends using all available Landsat 5, 7, and 8 images: a case study from Guangzhou, China (2000–2014). Remote Sens. Environ. 185, 243–257.

 https://doi.org/10.1016/j.heliyon.2019.e01478